The 2ν3 Raman overtone of sulfur hexafluoride: Absolute spectra, pressure effects, and polarizability properties

Michel Chrysos, Florent Rachet, David Kremer

The 2v3 Raman overtone of sulfur hexafluoride: Absolute spectra, pressure effects, and polarizability properties

M. Chrysos, F. Rachet, and D. Kremer

Citation: The Journal of Chemical Physics **140**, 124308 (2014); doi: 10.1063/1.4869097
View online: http://dx.doi.org/10.1063/1.4869097
View Table of Contents: http://scitation.aip.org/content/aip/journal/jcp/140/12?ver=pdfcov
Published by the AIP Publishing

The $2\nu_3$ Raman overtone of sulfur hexafluoride: Absolute spectra, pressure effects, and polarizability properties

M. Chrysos,[a] F. Rachet, and D. Kremer
LUNAM Université, Université d'Angers, CNRS UMR 6200, Laboratoire MOLTECH-Anjou, 2 Bd Lavoisier, 49045 Angers, France

(Received 9 February 2014; accepted 6 March 2014; published online 24 March 2014)

Of the six normal vibrations of SF_6, ν_3 has a key role in the mechanisms of radiative forcing. This vibration, though inactive in Raman, shows up through the transition $2\nu_3$ allowing for a complementary view on the asymmetric stretch of the molecule. Here, we look back into this topic, which has already caught some interest in the past but with some points been left out. We make a systematic incoherent-light-scattering analysis of the overtone with the use of different gas pressures and polarization orientations for the incident beam. Absolute-scale isotropic and anisotropic spectra are reported along with natural and pressure-induced widths and shifts, and other spectral features such as the peaks corresponding to the (experimentally indistinguishable) interfering channels E_g and F_{2g} hitherto seen solely as two-photon IR-absorption features. We make the first-ever prediction of the SF_6 polarizability second derivative with respect to the ν_3-mode coordinate and we develop a heuristic argument to explain why the superposition of the three degenerate stretching motions that are related to the ν_3 mode cannot but generate a polarized Raman band. © *2014 AIP Publishing LLC*. [http://dx.doi.org/10.1063/1.4869097]

I. INTRODUCTION

With a Global Warming Potential (GWP) of about 22 000,[1] sulfur hexafluoride is the most powerful of the Kyoto-protocol greenhouse gases.[2] The recent findings by NASA scientists that the absorbed infrared radiation by molecules having several F atoms bond to the same central X atom scales quadratically with the number of fluorine atoms[3] are an indirect confirmation of that property. This conclusion underlines the importance of reliable calculations of X–F bond-dipole derivatives for such molecules, since those quantities are now known to increase linearly with the number of fluorines.[3] It also stresses the significance of accurate values for the polarizability derivatives, which participate in the polarization mechanisms of SF_6 albeit do not enter directly GWP calculations.

Aside from Maroulis's seminal paper,[4] little is known on the polarizability derivatives of SF_6. Recently, a prediction of $\partial^2\bar{\alpha}/\partial q_5^2$ was made by our group for the "scissoring" mode of that molecule on the basis of high-sensitivity Raman experiments on the $2\nu_5$ overtone.[5] Yet the poor accuracy of the existing data for cubic force constants involving bending modes[6,7] of SF_6 prevented us from giving an unambiguous value for that derivative (even though a formula involving k_{155} as a free parameter was also given therein,[5] which will allow for a more reliable estimate of the derivative whenever a more reliable input for k_{155} comes out).

Among the six normal modes of sulfur hexafluoride, ν_3 is the only stretching vibration to generate a transition directly involved in the radiative forcing.[8] At least two studies, employing high-resolution spectroscopy, have been devoted to the infrared spectrum of that IR-active fundamental.[9,10] In a different context entirely, collision-induced Raman or hyper-Rayleigh processes involving sulfur hexafluoride have aroused keen interest in scientists in the last two decades,[11–16] reviving interest both in collision-induced processes[17–20] and in vibrational molecular spectroscopy.[21–23] More recently, SF_6 became the molecule of choice for testing a new spectroscopic probe, which uses impulsive stimulated Raman scattering and coherent electrons from high harmonic generation to monitor molecular dynamics.[24] Since few weeks, SF_6 is again in the forefront after the use of new cryogenic multipass cells, in high-resolution absorption experiments, which allowed for resolving its ever-challenging ν_6 forbidden band.[25] Here, prompted by our recent studies on the $2\nu_5$ spectra,[5,26] we employ incoherent Raman spectroscopy to detect the first overtone of the ν_3 vibration and to circumvent the handicap of the Raman inactivity of the ν_3 fundamental transition. Our work is a threefold advancement on an issue of vibrational Raman spectroscopy on which much has been accomplished[27,28] but on which the last is yet to be heard. First, it shows how to make a systematic, successful Raman analysis of the two overtone spectra (isotropic and anisotropic) with the use of two complementary yet independent light-scattering experiments that employ different polarizations for the incident beam, and with a series of experimental runs for various gas pressures. Accurate absolute-calibrated profiles along with their natural and pressure-induced band widths and shifts are reported for the two spectral components and a number of interesting features are revealed. Among other observations, the signature of the two channels E_g and F_{2g} is clearly distinguished on the anisotropic spectrum, a feature thus far only observed through two-photon IR-absorption spectroscopy[29] and computationally accessed by using a symmetrized

[a]Electronic mail: michel.chrysos@univ-angers.fr

local-mode basis.[30] From our observations and reliable data for the cubic force constant[6,7] k_{133}, a prediction for the second polarizability derivative $\partial^2\bar{\alpha}/\partial q_3^2$ is made, which is expected to be an accurate value for that property. Note that values for the force constants of SF_6 related to stretching of the S–F bond, such as k_{133}, are believed reliable, a fact also attested to by the good agreement between calculated ($k_{133} = -55.4$ cm^{-1}, Ref. 6; -56.75 cm^{-1}, Ref. 7) and measured values (-55.4 cm^{-1}, Ref. 6; -56.25 cm^{-1}, Ref. 7). Such constants are also known to take large values as compared to constants for stretch-bend or pure bend motions, and therefore are expected to significantly add to (or subtract from) the harmonic polarizability matrix-elements.

Finally, a heuristic argument is briefly outlined at the end of the article to explain the polarization properties of the scattered light for the $2\nu_3$ band.

II. THE EXPERIMENT IN BRIEF

The description of our experimental setup has been given in recent[5,26] and other publications[31–33] and will be skipped. We only recall (i) that the scattering intensities were recorded at an angle of 90° from the incident beam, (ii) that the polarization of this beam was chosen to be perpendicular ($\perp$) or parallel ($\parallel$) to the scattering plane, at will, and (iii) that, for either polarizations, the scattering signal (counts/s) was recorded at a fixed temperature, $T = 294.5 \pm 1$ K, and over a wide range of Raman wave numbers ν and gas densities ρ.

We remind the reader that the only way to reliably access physically meaningful light-scattering spectra, especially for weak bands, is to respect a stiff protocol, such as the one established by our group more than a decade ago, in which independent polarizations for the incident beam are used along with a series of independent runs for different gas-density values.[31,34–37] In the present study, we ran, for each polarization of the incident beam, 10 independent experiments for the following 10 values of gas density: 2, 3, 5, 7, 9, 11, 13, 15, 17, and 19 amagat (i.e., for gas pressures amounting to 2.13, 3.15, 5.12, 6.98, 8.74, 10.40, 11.95, 13.41, 14.77, and 16.03 bars). Calibration of the Raman signals on an absolute scale was made by means of the $S_0(1)$ rotational line of molecular hydrogen, ensuring, for each value of ρ, conversion to absolute spectral quantities $S_i(\rho, \nu)$ (with $i = \perp$ or $\parallel$) and $I_i(\nu) = S_i(\rho, \nu)/\rho$ (measured in units of cm^3 amagat and cm^3, respectively). The use of $S_i(\rho, \nu)$ helps the reader distinguish the whole series of spectra for the various values of ρ on the same graph. The intensity $I_i(\nu)$ only weakly depends on ρ, a dependence revealing the pressure effects of the spectrum. Note that the way in which the spectral widths and shifts in the observed bands depend on the gas density is expected to be linear, and its extrapolation to the $\rho = 0$ limit allows for revealing the natural characteristics of the band. Let us finally point out that in the only previous works on this overtone,[27,28] a fixed polarization ($\perp$) had been used for the incident beam, which had unavoidably restricted the recorded spectra to their polarized $I_\perp$ components. It is nevertheless remarkable that (as far as integrated intensities are concerned) the agreement between the previous results and the ones reported here is from good to excellent (see Table II).

After combination of the two intensities $I_\parallel(\nu)$ and $I_\perp(\nu)$ with appropriate linear expressions to take into account the aperture of the output beam, isotropic, I_{iso}, and anisotropic, I_{ani}, spectra are deduced, which tell us about the transition matrix-elements of the SF_6 polarizability invariants $\bar{\alpha}$ and $\Delta\alpha$, respectively, and reveal spectral features directly related to the symmetry classes of the overtone.

III. NOTIONS OF GROUPS AND SYMMETRY CLASSES

To go deeper into this statement, the $2\nu_3$ overtone expands as a sum of symmetry classes $A_{1g} \oplus E_g \oplus F_{2g}$, each of which is associated with certain polarizability components, as follows:[23]

$$\begin{aligned} A_{1g}&: \quad \alpha_{xx} + \alpha_{yy} + \alpha_{zz}, \\ E_g&: \alpha_{xx} + \alpha_{yy} - 2\alpha_{zz},\ \alpha_{xx} - \alpha_{yy}, \\ F_{2g}&: \quad \alpha_{xy},\ \alpha_{yz},\ \alpha_{zx}\ . \end{aligned}$$

The isotropic spectrum $I_{iso}(\nu)$ is generated by the mean polarizability $\bar{\alpha}$ and corresponds to the component A_{1g}. The anisotropic spectrum $I_{ani}(\nu)$ is generated by the anisotropy $\Delta\alpha$ and corresponds to components E_g and F_{2g}. As a result, there are two sublevels in the anisotropic overtone, which are indistinguishable experimentally, even though the symmetry restrictions to which the transition matrix-elements obey allow for substantial simplifications. The A_{1g} component is associated with value $l = 0$ for the vibrational angular momentum and with the combination $(v_{3,a}, v_{3,b}, v_{3,c}) = (2, 0, 0)$ for the vibrational quantum numbers of the final state because ν_3 is a triply degenerate mode. As for the E_g and F_{2g} components, both are associated with the value $l = 2$ but go with the combinations (2, 0, 0) and (1, 1, 0), respectively. The position of component A_{1g} was clearly localized on our isotropic spectrum. Thanks to our highly sensitive experiment, also the peaks of the two sub-bands corresponding to E_g and F_{2g} components were discerned on the top of the anisotropic spectrum, even though the main bodies of the two sub-bands were mixed up with each other as expected. Particularly gratifying was the fact that, despite the low resolution of our equipment, the positions of those three peaks agree well with results from eigenvalue calculations[30] as well as with observations from highly resolved two-photon IR-absorption experiments, carried out decades ago[29,38] or repeated several years later in the framework of sub-Doppler IR-IR double-resonance studies using a sideband spectrometer.[39] The origin of the discrepancies between our Raman results and those of the IR-IR experiments may be related to the specificity of each physical process. If the anisotropic intensity of the overtone were to lie entirely with one of the E_g or F_{2g} channels, either of the two expressions would be true: $(\Delta\alpha)^2_{fi} = \frac{3}{2}\langle 002000|\,\alpha_{xx} - \alpha_{yy}\,|000000\rangle^2$ for E_g or $(\Delta\alpha)^2_{fi} = 9\,\langle 002000|\,\alpha_{xy}\,|000000\rangle^2$ for F_{2g}, when summed over degeneracy. Yet, the way in which the total intensity of the anisotropic spectrum is shared between these channels cannot be deduced experimentally. Below, only upper bounds are given for the quantities $\langle 002000|\alpha_{xy}|000000\rangle$ and $\langle 002000|\alpha_{xx} - \alpha_{yy}|000000\rangle$, assuming that either the E_g or F_{2g} species could give the dominant contribution to $(\Delta\alpha)^2_{fi}$.

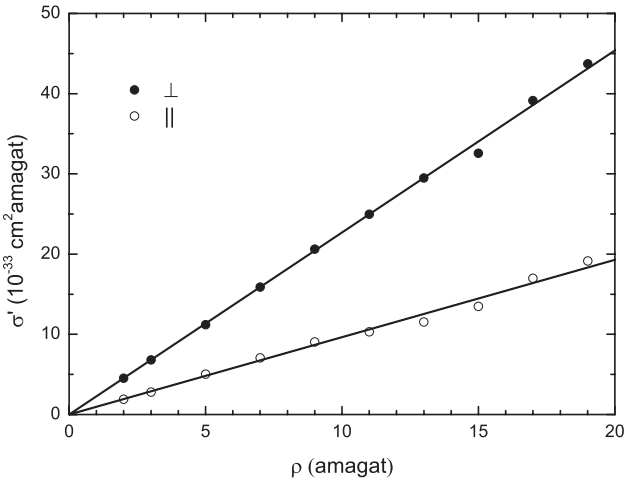

FIG. 1. Integrated signal $\sigma_i' = \int S_i(\rho, \nu)d\nu$ (in cm^2 amagat) as a function of density ρ (in amagat) for the two incident-beam polarizations $i = \perp$ (•) and $i = \parallel$ (○).

IV. RESULTS

For each of the ten values of ρ, frequency integration of $I_i(\nu)$ ($i = \perp, \parallel$) was carried out and the results were found to be insensitive to the values of ρ. This finding is evidence of spectra strictly pertaining to isolated SF_6 molecules, with no contamination by any binary, ternary, or higher-order collision-induced contributions or by parasitic effects due to foreign compounds. Figure 1 shows this property by illustrating the quantities $\sigma_\perp' = \int S_\perp(\rho, \nu)d\nu$ (filled symbols) and $\sigma_\parallel' = \int S_\parallel(\rho, \nu)d\nu$ (empty symbols) as a function of density. As anticipated above, the symbols associated with each spectral component are tightly packed along a straight line passing from zero. The property of such a well-defined straight line for each spectrum reveals that integrated intensities do not depend on ρ, and so neither do zeroth-order spectral moments. The absence of signal at the origin shows that there was no noise background.

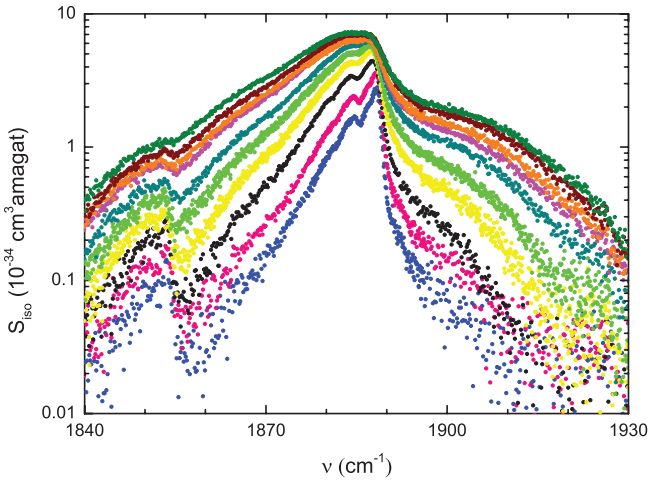

FIG. 2. Absolute-calibrated isotropic signal $S_{iso}(\rho, \nu)$ (in cm^3 amagat) in the region around 1888 cm^{-1} as a function of Raman frequency ν (in cm^{-1}), for ten values of ρ ranging from 2 to 19 amagat (in the upward direction).

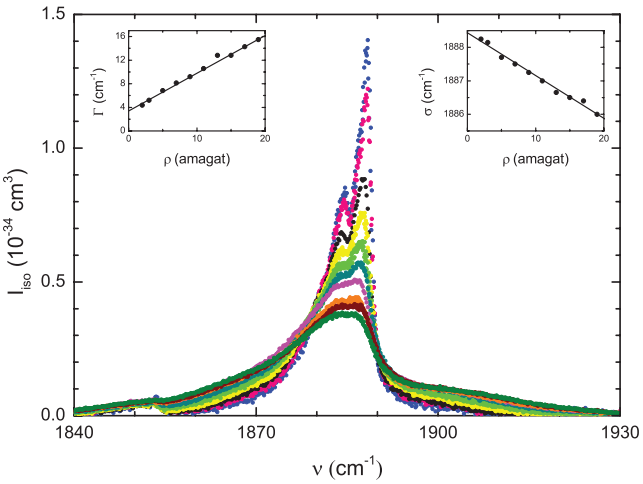

FIG. 3. Absolute-calibrated isotropic intensity I_{iso} (in cm^3) in the region around 1888 cm^{-1} as a function of Raman frequency ν (in cm^{-1}), for ten values of ρ ranging from 2 to 19 amagat. Same associations as the ones used in Fig. 2 are made between the values of density and the colors depicting the spectra. In the insets, the full width of the spectrum and the position of its maximum are shown as a function of ρ.

A. The isotropic spectrum

In Figures 2 and 3, calibrated isotropic spectra are shown, for the different values of gas density, as a function of ν. Figure 2 illustrates on a semi-logarithmic scale the function $S_{iso}(\rho, \nu)$. The spectral intensity $I_{iso}(\nu)$ is shown in Figure 3 on a linear scale. As a general remark, pressure effects are very pronounced in the isotropic spectrum, as attested to by the significant changes in the band shape of Figure 3 as the gas density is increased. The most pronounced peak seen on this figure corresponds to the position of branch Q of the $2\nu_3$ transition. The other pronounced peak located just before this transition is the branch Q of the hot band $\nu_6 + 2\nu_3 - \nu_6$. A simple calculation using the data reported in Table I of our previous article (Ref. 5) shows that, at room temperature, the population ratio between the levels (000000) and (000001) in SF_6 is $\frac{31.839}{17.490} = 1.82$, which exactly corresponds to the ratio of the two peak values upon extrapolation of the spectra to the $\rho \to 0$ limit.

At the far left side of the spectrum, a small structure (highlighted in the logarithmic plot of Figure 2) is discerned whose aspect is similar to the two pronounced bumps except for a scaling factor. This structure is identified as the $2\nu_3$ and $\nu_6 + 2\nu_3 - \nu_6$ transitions of the isotopomer $^{34}SF_6$. The peak intensity of this structure as compared to that of the main one well confirms this conclusion: their ratio amounts to $\simeq$20, a value corresponding to the concentration ratio[40] $\frac{95.02}{4.21}$ of sulfur

TABLE I. Full-width at $\frac{1}{\sqrt{e}}$-maximum, Γ (cm^{-1}), and position of the maximum, σ (cm^{-1}), for the isotropic and the anisotropic spectrum, as a function of ρ (in amagat).

	Isotropic	Anisotropic
Γ (cm^{-1})	$3.40(14) + 0.639(12)\rho$	$51.10(12) + 0.211(11)\rho$
σ (cm^{-1})	$1888.42(6) - 0.127(6)\rho$	$1892.39(28) - 0.271(23)\rho$

isotopes ^{32}S and ^{34}S. Furthermore, in accordance with qualitative expectations, the position of the overtone $2\nu_3$ for the isotopomer $^{34}SF_6$ shows a redshift of $-34.63(8)$ cm^{-1}, with respect to the overtone position of $^{32}SF_6$, that is about twice as great as the redshift value (-17.4163 cm^{-1}) observed for the corresponding ν_3 fundamentals in high-resolution jet-cooled IR-absorption experiments.[40] This isotopomeric band is also to be incorporated in the calculation of the overtone given that the polarizability matrix-elements for the two isotopomers are nearly equal and the concentration of the isotopomer ^{34}S in the cell is the same as in atmospheric SF_6.

In order to assess pressure effects on the isotropic spectrum, the band width and the position of the band maximum were carefully calculated for the various values of ρ. Significant pressure-broadening and redshift effects were found that obeyed a linear law in ρ. This is illustrated in the insets of Figure 3 and numerically given in Table I.

The main peak at the zero-density limit is located at the frequency $\nu = 1888.42(6)$ cm^{-1}. This value, which refers to the position of the A_{1g} component, compares well with the previously reported 1889.05 cm^{-1} and 1889.6 cm^{-1} values, obtained from two-photon IR-absorption experiments[29,38] and eigenvalue calculations,[30] respectively.

As a last remark about this spectrum, note that its shape closely resembles that of the recently studied $2\nu_5$ overtone,[5] in which the hot-band transition $\nu_6 + 2\nu_5 - \nu_6$ had again a significant role both in shape and in integrated intensity. At room temperature, the state (000001) of SF_6 is the second most populated level after the ground level.

A very important point to be stressed for the remainder of this article is that hot bands of the type $x + 2\nu_3 - x$ is an integral part of the overtone. By no means should these bands be excluded from the calculation of the overtone's spectral moment. This point, which has been adequately discussed in an article on the $2\nu_3$ overtone of CO_2 (Ref. 41, p. 194305-4), can be easily understood on the basis of the "principle of the communicating vessels," to depict metaphorically the transfer and the conservation of intensity between the principal transition $2\nu_3$ and the hot bands $x + 2\nu_3 - x$: If these bands were to be excluded from the overtone intensity, the remaining intensity would be temperature-dependent—and so too would be the resulting polarizability matrix-elements and derivatives, which is nonsensical.[42]

B. The anisotropic spectrum

We now turn our attention to the anisotropic spectrum of the overtone. At first sight this spectrum seems less sensitive to density variations than it was the isotropic spectrum. Here, the shape is strictly Gaussian whatever the density, yet observable broadening affects appear along with some shift of the peak values, both obeying linear density laws.

Figures 4 and 5 show, for the different values of gas density, the calibrated anisotropic spectra of the overtone as a function of ν. Figure 4 illustrates the function $S_{ani}(\rho, \nu)$, on a linear scale. The spectral intensity $I_{ani}(\nu)$ is shown in Figure 5. Apart from the clearly Gaussian shape of the spectrum, there is another interesting feature in this profile: Two spikes appear on the top of this spectrum, which are the distinctive marks

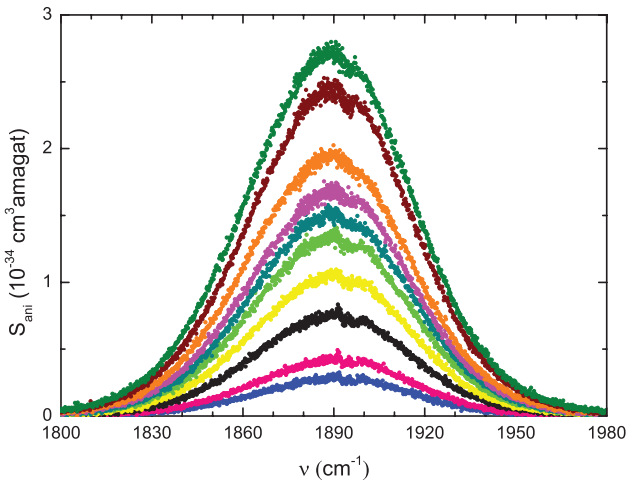

FIG. 4. Same as in Fig. 2 but for the anisotropic signal. The scale used here is linear.

of sublevels E_g and F_{2g}. Their positions, 1892.4(3) cm^{-1} and 1895.1 cm^{-1}, are close to the values of the literature, 1891.60 and 1896.53 cm^{-1}, respectively, obtained from two-photon IR absorption experiments.[29] They are also close to the calculated eigenvalues 1889.6 and 1895.6 cm^{-1}, respectively.[30] The discrepancies observed may have a physical origin related to the specificity of the process. Pressure effects are again shown as insets.

Figure 6 illustrates, for an arbitrary value of gas density, the quality of the Gaussian profile for the anisotropic spectrum. Thanks to such best fits, the pressure effects were again determined and found to satisfy a linear density law both for the band width and for the shift of the band maximum. The width of the anisotropic spectrum turns out to be about 15 times the width of its isotropic counterpart.

Table I gathers the pressure band broadening and shift density-laws for the isotropic and the anisotropic spectrum of the overtone. For both spectra, a redshift of the band maximum is observed, which for the anisotropic spectrum is twice as great as it is for the isotropic spectrum. Both spectra are broadened by pressure but the effect in the isotropic component is three times more substantial than it is for the

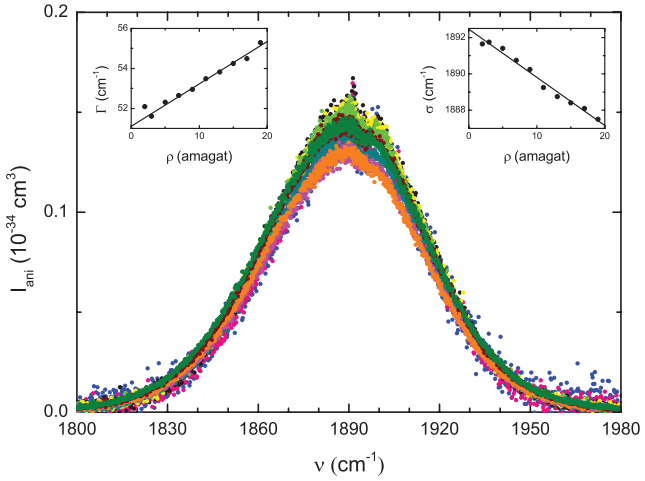

FIG. 5. Same as in Fig. 3 but for the anisotropic intensity.

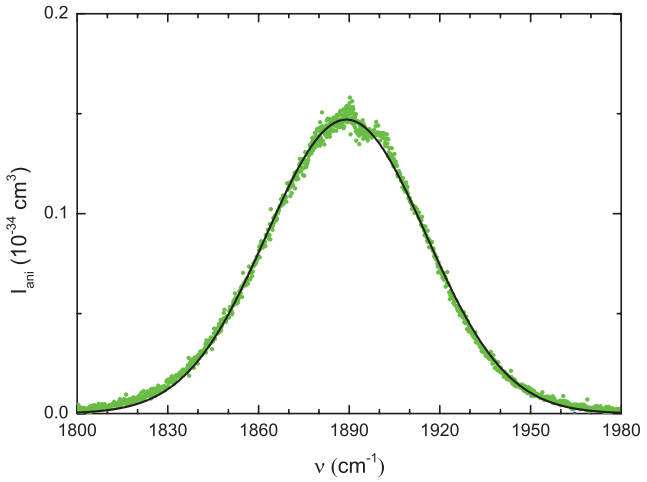

FIG. 6. Anisotropic intensity obtained experimentally (symbols) and its best fit with a Gaussian profile for an arbitrary value of gas density.

anisotropic component. All laws were found to be linear in density with a very low dispersion of the data points around the best fit curves. The insets of Figures 3 and 5 illustrate this property. Symbol Γ denotes full-width at $1/\sqrt{e}$-maximum; σ denotes the position of the maximum.

C. Depolarization ratio and spectral moment

Figure 7 shows the depolarization ratio $\eta(\nu)$ of the overtone as a function of Raman frequency ν, for three representative values of gas density. The overtone is highly polarized close to the band center and this trend is enhanced as density is decreased. Away from the center, the band becomes quickly depolarized. The presence of the isotopomer $^{34}SF_6$ is clearly seen at the left side of the figure. The striking similarity between the two $^{32,\,34}SF_6$ isotopic structures (except for a scale factor) is better shown here than in Figure 3.

An integrated depolarization ratio was also calculated for each density, and its average value turned out to be η_{int} = 0.43(2). This result is in marginal agreement with the number $\eta_{int} = \frac{2\eta_s}{1+\eta_s} = 0.46$ deduced from the value $\eta_s \simeq 0.30$ reported by Holzer and Ouillon.[27] The $2\nu_3$ overtone, though still qualified as a "polarized band," is definitely far less polarized than the $2\nu_5$ overtone.[26]

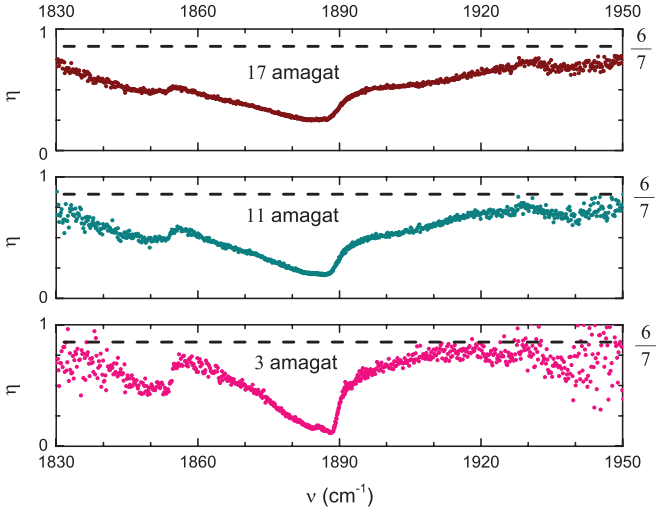

FIG. 7. Depolarization ratio $\eta(\nu)$ as a function of ν (in cm^{-1}) for the representative gas density values 3, 11, and 17 amagat.

TABLE II. Isotropic and anisotropic zeroth-order (M_0) spectral moments in units of cm^6. Comparison with results from previous works is made.

M_0 (cm^6)	This work	Previous works
Isotropic	8.12(50) × 10^{-54}	8.25 × 10^{-54}[a]
		6.10 × 10^{-54}[b]
Anisotropic	5.04(32) × 10^{-53}	5.93 × 10^{-53}[a]
		4.58 × 10^{-53}[b]

[a]Shelton and Ulivi, Ref. 28.
[b]Holzer and Ouillon, Ref. 27.

Isotropic and anisotropic zeroth-order spectral moments, M_0, were also calculated, and their values (in cm^6) are gathered in Table II along with the M_0 values from previous studies. Note that in none of the past studies was the incident-beam polarization oriented in other than the ⊥ direction. The experimental uncertainty (values in parentheses) is the sum of the statistical errors due to the linear regression and of the 6% systematic errors in the calibration procedure.

D. The matrix-elements $(\Delta\alpha)_{fi}$ and $(\bar{\alpha})_{fi}$

In view of the results gathered in Table II and of the discussion in Sec. III, absolute values of transition matrix-elements (002000) ← (000000) for the mean polarizability $\bar{\alpha}$ and anisotropy $\Delta\alpha$ along with values for the upper bounds of the matrix-elements of the two experimentally indistinguishable anisotropy components $(\alpha_{xx} - \alpha_{yy})$ and α_{xy} can be derived. These are gathered in Table III.

E. The second derivatives

Starting from the zeroth-order moment, M_0, it is now possible to deduce the harmonic second derivative $\partial^2\bar{\alpha}/\partial q_3^2$, by means of two expressions given in Ref. 5 [Eqs. (9) and (12) therein] whenever adapted to the case $i = 3$.

Because of the Raman inactivity of transition ν_3, one has $\partial\bar{\alpha}/\partial q_3 = 0$. As for the first derivatives in the summation of the second expression, $\partial\bar{\alpha}/\partial q_1$ is the only nonzero term. This is because the transitions ν_4 and ν_6 are Raman-inactive, while ν_2 and ν_5 are totally depolarized, which means that ν_1 is the only Raman-active transition to be totally polarized. As a consequence of this, the harmonic derivative reads

$$\frac{\partial^2\bar{\alpha}}{\partial q_3^2} = \pm\sqrt{\frac{8}{3\gamma_3(T)}M_0} - 2k_{133}\frac{\omega_1}{4\omega_3^2 - \omega_1^2}\frac{\partial\bar{\alpha}}{\partial q_1}. \quad (1)$$

Full account of the hot bands corresponding to the ladder $n\nu_3 - (n-2)\nu_3$ with $n = 2, 3, 4, \ldots$ was taken through the hot-band factor $\gamma_i(T)$ (with $i = 3$, $T = 294$ K). Its value for the $2\nu_3$ band amounts to only 1.02. On the other hand, let us emphasize again that hot bands corresponding to excited

TABLE III. Absolute values of matrix-elements for mean polarizability $\bar{\alpha}$ and polarizability anisotropy $\Delta\alpha$ along with values for the upper bounds of matrix-elements $(\alpha_{xx} - \alpha_{yy})$ and α_{xy}. Values from previous studies are also given. All values are in cm^3.

$\lvert\langle 002000\rvert\Delta\alpha\rvert 000000\rangle\rvert$	$\lvert\langle 002000\rvert\alpha_{xx} - \alpha_{yy}\rvert 000000\rangle\rvert$	$\lvert\langle 002000\rvert\alpha_{xy}\rvert 000000\rangle\rvert$	$\lvert\langle 002000\rvert\bar{\alpha}\rvert 000000\rangle\rvert$
E_g, F_{2g}	E_g	F_{2g}	A_{1g}
$7.03(22) \times 10^{-27}$	5.74×10^{-27}	2.34×10^{-27}	$2.82(9) \times 10^{-27}$
7.62×10^{-27}[a]	6.23×10^{-27}[a]	2.54×10^{-27}[a]	2.84×10^{-27}[a]
6.70×10^{-27}[b]			2.45×10^{-27}[b]

[a]Shelton and Ulivi, Ref. 28.
[b]Holzer and Ouillon, Ref. 27.

modes other than the mode ν_3, such as $\nu_6 + 2\nu_3 - \nu_6$, etc., should instead enter the calculation of the overtone intensity in order to preserve the temperature independence of the resulting matrix-elements and thus of the derived polarizability derivatives.

Table IV gathers the values of the effective anharmonic derivative $(\partial^2\bar{\alpha}/\partial q_3^2)_{anh}$ along with the derived values of the harmonic property $\partial^2\bar{\alpha}/\partial q_3^2$ at the equilibrium position in units of $10^{-2}\ a_0^3$ (a_0 is the Bohr radius). The different values of $\partial^2\bar{\alpha}/\partial q_3^2$ corresponding to the same $(\partial^2\bar{\alpha}/\partial q_3^2)_{anh}$ value arise from the different entry data for k_{133} and $\partial\bar{\alpha}/\partial q_1$. For derivative conversions, see the note of Ref. 44. The fact that the sign difference in the input anharmonic derivative results in values of $\partial^2\bar{\alpha}/\partial q_3^2$ that differ both in the sign and in the order of magnitude leaves room for cheap *ab initio* calculations to decide between the two signs and to numerically assess the actual value of the harmonic property.

As regards the derivatives $\frac{\partial^2\Delta\alpha}{\partial q_{3,a}^2}$ and $\frac{\partial^2\Delta\alpha}{\partial q_{3,a}\partial q_{3,b}}$ ($q_{3,a}$ and $q_{3,b}$ denote any two of the three dimensionless normal coordinates for the triply degenerate ν_3 mode), the data are not sufficient to deduce their values from our observations because the two sub-bands E_g and F_{2g} cannot be discerned experimentally from the anisotropic spectrum. Yet, given that these components are associated with the stretching quantum numbers $(v_{3,a}, v_{3,b}, v_{3,c}) = (2, 0, 0)$ and $(1, 1, 0)$, respectively, the quantities $\frac{\partial^2\Delta\alpha}{\partial q_{3,a}^2}$ and $\frac{\partial^2\Delta\alpha}{\partial q_{3,a}\partial q_{3,b}}$ will be reduced to two separated terms involving $\frac{\partial^2(\alpha_{xx}-\alpha_{yy})}{\partial q_{3,a}^2}$ and $\frac{\partial^2\alpha_{xy}}{\partial q_{3,a}\partial q_{3,b}}$, depending on whether it is the E_g or the F_{2g} component that is treated, respectively. Unfortunately, Raman spectroscopy offers no possibility to separate these two derivatives in the sum.

Note that to calculate $\frac{\partial^2(\alpha_{xx}-\alpha_{yy})}{\partial q_{3,a}^2}$ and $\frac{\partial^2\alpha_{xy}}{\partial q_{3,a}\partial q_{3,b}}$, one needs the matrix-elements for the two sub-bands, as well as anharmonic corrections that involve cubic force constants[26] k_{233} and k_{335} and first harmonic derivatives with respect to q_2 and q_5. No data for any direct or cross second derivative of $(\alpha_{xx} - \alpha_{yy})$ or α_{xy} are available in the existing literature. The known values for the constant k_{233} are expected to be accurate to within <10% (for they involve only stretching modes). The ones for k_{335} are less reliable. Table V gathers values for the cubic force constants (in cm^{-1}) entering the calculation of the second polarizability derivatives of ν_3. These values have been taken from previous experimental and theoretical studies. One explanation for the large discrepancy between the two k_{335} values -4.58 and $-2.05\ cm^{-1}$ reported in Ref. 7 is that the latter has been predicted from the harmonic force-field.[7] Note that the data for the cubic force constants reported in the literature sometimes refer to C_{133}, C_{233}, and C_{335}, or to ϕ_{133}, ϕ_{233}, and ϕ_{335}, but their conversion to k_{133}, k_{233}, and k_{335} is possible through the expressions $k_{133} = \frac{\phi_{133}}{2!}$, $k_{233} = \frac{\phi_{233}}{2!}$, $k_{335} = \frac{\phi_{335}}{2!}$, and $\phi_{133} = 2C_{133}$, $\phi_{233} = \sqrt{\frac{8}{3}}C_{233}$, $\phi_{335} = C_{335}$. The expressions relating nomenclature C to nomenclature ϕ in SF_6 have been given in Ref. 45 (Table 2, therein). Confusions between the meaning of k and ϕ are often witnessed in relationships involved in anharmonicity corrections. In this context, see a comment published recently.[46]

TABLE IV. Values of $(\partial^2\bar{\alpha}/\partial q_3^2)_{anh}$ and $\partial^2\bar{\alpha}/\partial q_3^2$, at the equilibrium position, in units of $10^{-2}a_0^3$. The different values of $\partial^2\bar{\alpha}/\partial q_3^2$ corresponding to the same $(\partial^2\bar{\alpha}/\partial q_3^2)_{anh}$ value arise from the different entry data for k_{133} and $\partial\bar{\alpha}/\partial q_1$.

$\left(\frac{\partial^2\bar{\alpha}}{\partial q_3^2}\right)_{anh}$ $(10^{-2}\ a_0^3)$	$\frac{\partial^2\bar{\alpha}}{\partial q_3^2}$ $(10^{-2}\ a_0^3)$			
3.11	5.95[a,b]	5.84[a,c]	5.90[b,d]	5.80[c,d]
−3.11	−0.27[a,b]	−0.38[a,c]	−0.32[b,d]	−0.42[c,d]

[a]$k_{133} = -56.25\ cm^{-1}$ (expt.), Ref. 7.
[b]$\partial\bar{\alpha}/\partial q_1 = 0.975a_0^3$ (expt.), Ref. 43.
[c]$\partial\bar{\alpha}/\partial q_1 = 0.937a_0^3$ (*ab initio*), Ref. 4.
[d]$k_{133} = -55.4\ cm^{-1}$ (calculations), Ref. 6.

V. A HEURISTIC ARGUMENT

Let us now present a heuristic argument to justify why the $2\nu_3$ band is polarized. This argument, initially reported in Ref. 32 to show that the $2\nu_3$ overtone of CO_2 is a depolarized band, runs as follows. In the asymmetric stretching of CO_2, the two oxygen atoms spend most of their time

TABLE V. Cubic force constants (in cm^{-1}) entering the calculation of the second polarizability derivatives. In the last row, the values and their uncertainties (shown in parentheses) enable a quick inventory of the different results obtained with various theoretical assumptions in Ref. 6.

Pure stretch		Stretch-bend
k_{133}	k_{233}	k_{335}
−56.25[a]	−87.7[a]	−4.58[a]
−56.75[b]	−86.1[b]	−2.05[b]
−55.4[c]	−89.1[c]	−5.0[c]
−55.4(1)[d]	−85(2)[d]	−6.4(2)[d]

[a]Reference 7 (expt).
[b]Reference 7 (calculations).
[c]Reference 6 (expt).
[d]Reference 6 (calculations).

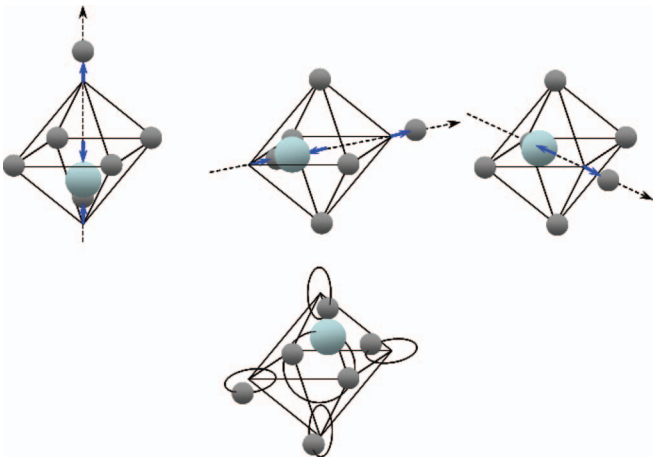

FIG. 8. Sketching SF_6 in the ν_3 vibration. The three cartoons (upper row) depict the three stretching motions along the three S–F–S axes (dashed-line arrows) for the triply degenerate stretching ν_3 vibration of the molecule. Superposition of the three independent motions, each with arbitrary phase, leads to ellipsoidal motions for the vibrating atoms. The two-dimensional ellipses of motion that result from the combination of just two of the ν_3 components are shown in the single cartoon (lower row).

close to the turning points, i.e., in positions of two unequal C–O lengths. As there are two equivalent such configurations, depending on whether it is the one or the other oxygen which is closer to carbon, the molecule scatters the radiation like an effective binary system. But (collision-induced) light-scattering by binary systems is known to be a process primarily depolarized,[17,47] which is exactly what was observed with the $2\nu_3$ band of CO_2 ($\frac{M_0^{ani}}{M_0^{iso}} \simeq 420$, see Ref. 33). Does this argument also apply to the $2\nu_3$ band of SF_6? Because of its triple degeneracy, the ν_3 vibration in SF_6 is not in all aspects the same as the ν_3 vibration of CO_2, even though in both vibrations there are three aligned atoms to stretch asymmetrically. As a result, the atoms in SF_6 undergo a superposition of three stretching motions (one per F–S–F axis), each with a different phase, and the resulting picture resembles an effective spherical particle. This property shows that the $2\nu_3$ of SF_6 is a polarized band ($\frac{M_0^{ani}}{M_0^{iso}} \simeq 6$, see Table II), in agreement with the general statement that spherical systems generate polarized light-scattering spectra. This is illustrated in Figure 8. In the first row of this figure, three cartoons are sketched to depict the three orthogonal stretch motions in the ν_3-vibrating molecule. The fourth cartoon shown alone depicts the combined motion between two of the former asynchronous motions. The resulting motion brings about vibrational momentum l and Coriolis couplings—a situation having little in common with the non-degenerate ν_3 vibration of CO_2.[48]

VI. SYNOPSIS

We reported a rather exhaustive analysis of the SF_6 $2\nu_3$ overtone at room temperature. This overtone arises from electrical anharmonicity and is allowed in Raman even though its fundamental transition is not. It was detected with light-scattering equipment of unprecedented sensitivity and with use of a meticulous protocol, involving two different polarizations for the incident beam and a series of ten different gas pressures. This enabled access to a multitude of hitherto unknown properties and features, such as frequency-resolved absolute isotropic and anisotropic spectra at the low density limit, pressure broadening and shift effects, and subtle structures such as the positions of the E_g and F_{2g} sub-bands relevant to the anisotropic spectrum, which (along with the all-symmetrical A_{1g}) were so far only accessible through multiphoton infrared absorption. Our study also permitted a prediction of the second derivative of the molecule's mean polarizability as an attempt to fill a gaping hole in the literature. Comparative analysis with the few data found in the two previous Raman studies on this overtone was made, and the agreement observed is a further validation of our approach and a guarantee for its success. A number of other findings were also discussed in relation with the role of the hot bands around the main transition, the presence of isotopomers, the degree of accuracy of the anharmonicity cubic force constants, and the role of this overtone in general as a means to better understand the inner workings of the ν_3 asymmetric stretching of SF_6. This vibration is the main cause of radiative forcing by this molecule, whose global warming potential is the largest of all Kyoto-protocol greenhouse gases.

[1] One kilogram of SF_6 is equivalent to 22.8 metric tons of CO_2 on a 100-year time horizon.
[2] M. K. W. Ko, N. D. Sze, W.-C. Wang, G. Shia, A. Goldman, F. J. Murcray, D. G. Murcray, and C. P. Rinsland, J. Geophys. Res. **98**, 10499, doi:10.1029/93JD00228 (1993).
[3] P. P. Bera, J. S. Francisco, and T. J. Lee, J. Phys. Chem. A **113**, 12694 (2009).
[4] G. Maroulis, Chem. Phys. Lett. **312**, 255 (1999).
[5] D. Kremer, F. Rachet, and M. Chrysos, J. Chem. Phys. **138**, 174308 (2013).
[6] B. J. Krohn and J. Overend, J. Phys. Chem. **88**, 564 (1984).
[7] D. P. Hodgkinson, J. C. Barrett, and A. G. Robiette, Mol. Phys. **54**, 927 (1985).
[8] In this vibration, two fluorines and the central S atom, aligned together, undergo asymmetric stretching motion along their common axis. The symmetry coordinate of the ν_3 vibration reads $\frac{R_1-R_2}{\sqrt{2}}$, where R_1 and R_2 designate the elongations of the two diametrically opposite stretched S–F bonds. A similar expression, with R_1 and R_2 as the elongations of the two C–O bonds, enters the calculations in the case of the ν_3 vibration of CO_2.
[9] B. Bobin, Ch. J. Bordé, J. Bordé, and Ch. Bréant, J. Mol. Spectrosc. **121**, 91 (1987).
[10] O. Acef, Ch. J. Bordé, A. Clairon, G. Pierre, and B. Sartakov, J. Mol. Spectrosc. **199**, 188 (2000).
[11] T. Bancewicz, J.-L. Godet, and G. Maroulis, J. Chem. Phys. **115**, 8547 (2001).
[12] J.-L. Godet, F. Rachet, Y. Le Duff, K. Nowicka, and T. Bancewicz, J. Chem. Phys. **116**, 5337 (2002).
[13] Y. Le Duff, J.-L. Godet, T. Bancewicz, and K. Nowicka, J. Chem. Phys. **118**, 11009 (2003).
[14] I. A. Verzhbitskiy, M. Chrysos, F. Rachet, and A. P. Kouzov, Phys. Rev. A **81**, 012702 (2010).
[15] M. Chrysos and I. A. Verzhbitskiy, Phys. Rev. A **81**, 042705 (2010).
[16] I. A. Verzhbitskiy, M. Chrysos, and A. P. Kouzov, Phys. Rev. A **82**, 052701 (2010).
[17] L. Frommhold, Adv. Chem. Phys. **46**, 1 (1981).
[18] *Collision- and Interaction-Induced Spectroscopy*, edited by G. C. Tabisz and M. N. Neuman (Kluwer, Dordrecht, 1995).
[19] T. Bancewicz, Y. Le Duff, and J.-L. Godet, Adv. Chem. Phys. **119**, 267 (2001).
[20] J.-M. Hartmann, C. Boulet, and D. Robert, *Collisional Effects on Molecular Spectra. Laboratory Experiments and Models, Consequences for Applications* (Elsevier, Amsterdam, 2008).
[21] G. C. Tabisz, in *Molecular Spectroscopy: A Specialist Periodical Report*, edited by R. F. Barrow, D. A. Long, and J. Sheridan (Chemical Society, London, 1979), Vol. 6, pp. 136–173.

[22]E. B. Wilson, Jr., J. C. Decius, and P. C. Cross, *Molecular Vibrations: The Theory of Infrared and Raman Vibrational Spectra* (Dover, New York, 1980).
[23]D. A. Long, *The Raman Effect. A Unified Treatment of the Theory of Raman Scattering by Molecules* (Wiley, Chichester, UK, 2002).
[24]N. L. Wagner, A. Wüest, I. P. Christov, T. Popmintchev, X. Zhou, M. M. Murnane, and H. C. Kapteyn, Proc. Natl. Acad. Sci. U.S.A. **103**, 13279 (2006).
[25]V. Boudon, L. Manceron, F. Kwabia Tchana, M. Loëte, L. Lago, and P. Roy, Phys. Chem. Chem. Phys. **16**, 1415 (2014).
[26]D. Kremer, F. Rachet, and M. Chrysos, J. Chem. Phys. **140**, 034308 (2014).
[27]W. Holzer and R. Ouillon, Chem. Phys. Lett. **24**, 589 (1974).
[28]D. P. Shelton and L. Ulivi, J. Chem. Phys. **89**, 149 (1988).
[29]C. W. Patterson, B. J. Krohn, and A. S. Pine, Opt. Lett. **6**, 39 (1981).
[30]L. Halonen and M. S. Child, J. Chem. Phys. **79**, 559 (1983).
[31]F. Rachet, Y. Le Duff, C. Guillot-Noël, and M. Chrysos, Phys. Rev. A **61**, 062501 (2000).
[32]M. Chrysos, I. A. Verzhbitskiy, F. Rachet, and A. P. Kouzov, J. Chem. Phys. **134**, 044318 (2011).
[33]M. Chrysos, I. A. Verzhbitskiy, F. Rachet, and A. P. Kouzov, J. Chem. Phys. **134**, 104310 (2011).
[34]F. Rachet, M. Chrysos, C. Guillot-Noël, and Y. Le Duff, Phys. Rev. Lett. **84**, 2120 (2000).
[35]Y. Le Duff, Phys. Rev. Lett. **90**, 193001 (2003).
[36]M. Chrysos, A. P. Kouzov, N. I. Egorova, and F. Rachet, Phys. Rev. Lett. **100**, 133007 (2008).
[37]S. Dixneuf, M. Chrysos, and F. Rachet, J. Chem. Phys. **131**, 074304 (2009).
[38]C. W. Patterson, R. S. McDowell, P. F. Moulton, and A. Mooradian, Opt. Lett. **6**, 93 (1981).
[39]M. Khelkhal, E. Rusinek, J. Legrand, F. Herlemont, and G. Pierre, J. Chem. Phys. **107**, 5694 (1997).
[40]V. Boudon, M. Hepp, M. Herman, I. Pak, and G. Pierre, J. Mol. Spectrosc. **192**, 359 (1998).
[41]I. A. Verzhbitskiy, A. P. Kouzov, F. Rachet, and M. Chrysos, J. Chem. Phys. **134**, 194305 (2011).
[42]Strictly, the interaction of the SF_6 molecules with the blackbody radiation of the surroundings is expected to lead to matrix-elements that are temperature-dependent. In this respect, there has been evidence since the mid-1990s of a temperature-dependent dipole polarizability, $\alpha(\omega, T)$, in rare gas atoms owing to a dynamic non-resonant Stark effect caused by blackbody radiation [U. Hohm and U. Trümper, Chem. Phys. **189**, 443 (1994)]. Such effects are too small to be observable at the temperature of our experiment.
[43]D. A. Long and E. L. Thomas, Trans. Faraday Soc. **59**, 1026 (1963).
[44]According to Maroulis,[4] "at MP2 level the dipole polarizability varies with the S–F bond length (symmetric stretch) as $[\alpha(R) - \alpha(R_0)]/e^2a_0^2E_h^{-1} = 25.38\Delta R + 13.72\Delta R^2 - 0.99\Delta R^3$, where $\Delta R/a_0 = (R_{S-F} - R_0)$ and R_0 is the experimental S–F separation." Upon conversion of $\frac{\partial\bar{\alpha}}{\partial\Delta R} = 25.38a_0^2$ to the derivative with respect to q_1, we obtain $\frac{\partial\bar{\alpha}}{\partial q_1} = 0.0369 \times 25.38 = 0.937a_0^3$. Similarly, the value $26.42a_0^2$ reported in Ref. 43 will be converted to $\frac{\partial\bar{\alpha}}{\partial q_1} = 0.975a_0^3$.
[45]D. P. Hodgkinson, R. K. Heenan, A. R. Hoy, and A. G. Robiette, Mol. Phys. **48**, 193 (1983).
[46]M. Chrysos and D. Kremer, Int. J. Quantum Chem. **113**, 2634 (2013).
[47]Y. Le Duff, A. Gharbi, and T. Othman, Phys. Rev. A **28**, 2714 (1983).
[48]More on this point about SF_6, UF_6, SiF_4, and CO_2, and their illustrations for degenerate modes and coupled vibrational motions, can be found in the popular-science article by R. S. McDowell, C. W. Patterson, and W. G. Harter, Los Alamos Sci. **4**, 38 (1982). Note in passing that the theoretical shape of the two-photon contribution to the spectrum of ν_3, based on an analysis of $3\nu_3$ and shown in the latter article (Fig. 12 upper panel, p. 60), provides the values 944.5, 945.8, and 947.7 cm^{-1} for the positions of the three main peaks; an interesting agreement with our findings, 1888.4, 1892.4, and 1895.1 cm^{-1}, is observed upon halving the latter values to make them correspond to the same frequency region as in single laser-photon absorption.